B1 PHASE SPATIAL PATTERN AT 7 TESLA: IMPACT ON B1 INHOMOGENEITIES WITH A HEAD TRANSCEIVE TRANSMISSION LINE ARRAY COIL

P-F. Van de Moortele[1], G. Adriany[1], C. Akgun[1], S. Moeller[1], J. Ritter[1], J. T. Vaughan[1], K. Ugurbil[1]
[1]CMRR/Radiology, University of Minnesota, Minneapolis, MN, United States

Introduction

RF penetration in human head is challenging at ultra high magnetic field (UHF); a bright center and a weak periphery have been reported with volume coils[1], while surface coils provide strong B1 in the periphery[2]. The intensity patterns observed with the volume coils are often referred to as "dielectric resonances", a view that conflicts with conclusions reached on modeling studies, where they have been ascribed to superposition of traveling and reflected waves[3]. Here we address this question experimentally, taking full advantage of a transceiver coil array that allows utilizing an identical coil structure as a volume transmit coil, multiple receive coils, or multiple single transmit surface coils.

Material and Methods

Experiments were performed on a 90-cm bore, 7T magnet (Magnex, Varian). We used an 8 channels transceiver array coil[4], consisting of eight transmission lines on a cylindrical holder. Transmit RF power was split with an 8-way power splitter. Phase increments of ~45 degrees between neighboring coils were set through cable lengths. We used an 8 channel digital receiver (Echotek).

Phantom data. GE images (TE/TR = 5ms/1s, flip = 15°) were obtained in an axial slice crossing the center of a 3 liter spherical flask, filled with 90mM NaCl saline water. Transmit B1 (**B1+**) profiles were mapped using a magnetization preparation pulse[1] (MPP) followed by ultrafast GE images with flip angle ~3°. MPP duration ranged from 0 to 3000μs. One image was acquired every 16 sec. This approach was used to map **B1+** either when transmitting through all 8 coil elements (one "volume coil" **B1+** map) or when transmitting through one element at a time (8 "surface coil" B1 maps). Once **B1+** is known, receive B1 profile (**B1-**) can be computed as well for each channel.

Human* data. Axial GE images of the brain were obtained transmitting through all 8 elements (volume transmit coil), collecting data on 8 channels simultaneously but separately (receive array).

Data Analysis

We call $\mathbf{p}_{r,j}$ the complex value of a voxel at location r measured in channel j. First, for each channel a global phase shift was applied in order to have a null phase in the phantom center. Second, complex data from all coils were summed (as has been suggested[5], but here *divided* by their magnitude) to obtain an estimation of a common phase term: $\varphi_{r,com}=\arg(\Sigma(\mathbf{p}_{rj}/|\mathbf{p}_{r,j}|))$, which was then removed from all data. The resulting phase corrected complex data (**PhCorrCpx**) of the 8 channels were summed in different ways: Sum of Magnitude image (**SofM**), Magnitude of Sum of complex images (**MofS**), root sum of squares (**RSS**).

Results and Discussion

(in all figures the color scale range is shown in brackets; a.u.=arbitrary unit)

Phantom. In **Fig. 1**, relative coil intensity profiles were obtained by dividing each channel magnitude by **SofM**. Note that this ratio does not exceed 0.56. The right-most image shows which of the 8 channels (one color per channel) contributes the most at a particular voxel. The twisted shape in *amplitude* is typical at UHF[6]. In this study we will focus on the associated *phase* pattern twist. **Fig. 2** shows a fundamental feature: **MofS** divided by **SofM** or by **RSS** shows considerable signal loss in the periphery while in the center **MofS**, **SofM** and **RSS** are equal (ratio=1). In order to see if complex interferences could explain this signal loss, we looked at the *relative* coil phase pattern: **Fig 3a** shows **PhCorrCpx** spatial phase pattern: first, it exhibits large phase excursions through the sample (over 2π within one channel). Second, when aligning all elements on 1 channel (here #3) by appropriate rotation (**Fig 3b**), a highly reproducible *relative* phase pattern is found. Third, in the periphery, the area closest to one channel is out of phase by up to π radians with respect to its nearest neighbors, naturally a perfect situation for destructive interference. Such interferences should also be reproduced by calculating the |**B1-**| map from the complex sum of all channels, rather than by adding the 8 individual |$\mathbf{B1}_j$**-**|maps shown in **Fig 4a**. This is demonstrated in **Fig 5**, where the ratio between such |**B1-**| maps shows again a substantial loss in the periphery while numbers are equal at the center. We hypothesized that individual coil $\mathbf{B1}_j$**+'s**, which are twisted in opposite direction[3] (**Fig 4b**), should also cancel each other through destructive interference. **Fig 6** shows that summing the 8 |$\mathbf{B1}_j$**+**| maps (obtained transmitting through one channel at a time) yields a final |**B1+**| clearly stronger in the periphery than in the center, while |**B1+**| obtained transmitting through 8 channels together is weaker in the periphery.

Human. We verified the same properties for **B1-** with a human brain. **Fig 7** shows that **SofM** has stronger signal in the periphery, which is lost for a large part in **MofS**. A spatial phase pattern is found again for **PhCorrCpx** in **Fig 8a**. In **Fig 8b** GE magnitude images show coil elements location.

CONCLUSION

Our results, with lossy samples, suggest that typical B1 patterns (strong center, weak periphery) observed with volume coils at UHF come to a large extent not from dielectric resonances but from interferences between different coil elements generating **B1** vectors in the sample that are not in phase. This is due to significant **B1** phase distortions at UHF. Relative coil phase patterns may provide a rationale for RF focusing algorithms when RF amplitude and phase can be modulated for different coil elements.

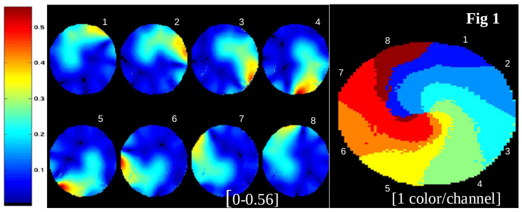

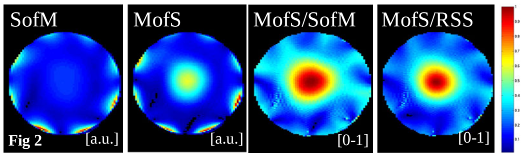

$$\sum_j^N \left|\vec{\mathbf{p}}_j\right| \qquad \left|\sum_j^N \vec{\mathbf{p}}_j\right| \qquad \left|\sum_j^N \vec{\mathbf{p}}_j\right| \div \sum_j^N \left|\vec{\mathbf{p}}_j\right| \qquad \left|\sum_j^N \vec{\mathbf{p}}_j\right| \div \sqrt{N \cdot \sum_j^N \left(\left|\vec{\mathbf{p}}_j\right|\right)^2}$$

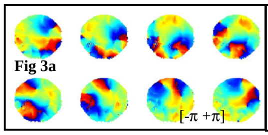

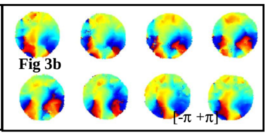

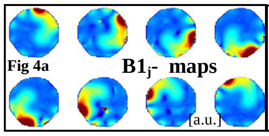

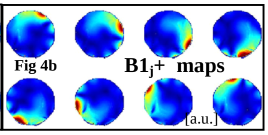

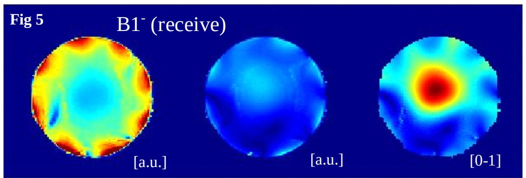

$$\sum_j^N \left|\vec{\mathbf{B}}^-_{1,j}\right| \qquad \left|\mathbf{B}^-_1\right| \textit{ from } \sum_j^N \vec{\mathbf{p}}_j \qquad \sum_j^N \left|\vec{\mathbf{B}}^-_{1,j}\right| \div \left|\mathbf{B}^-_1\right| \textit{ from } \sum_j^N \vec{\mathbf{p}}_j$$

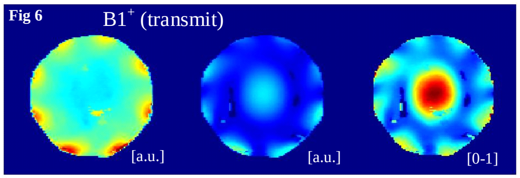

$$\sum_j^N \left|\vec{\mathbf{B}}^+_{1,j}\right| \qquad \left|\sum_j^N \vec{\mathbf{B}}^+_{1,j}\right| \qquad \left|\sum_j^N \vec{\mathbf{B}}^+_{1,j}\right| \div \sum_j^N \left|\vec{\mathbf{B}}^+_{1,j}\right|$$

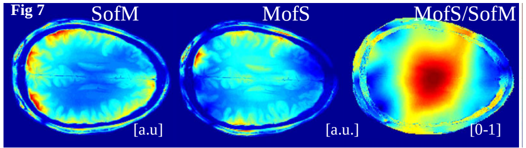

$$\sum_j^N \left|\vec{\mathbf{p}}_j\right| \qquad \left|\sum_j^N \vec{\mathbf{p}}_j\right| \qquad \left|\sum_j^N \vec{\mathbf{p}}_j\right| \div \sum_j^N \left|\vec{\mathbf{p}}_j\right|$$

Fig 8a

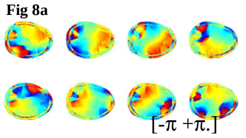

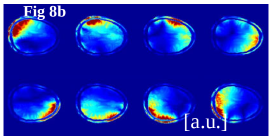

References: **1)** Vaughan JT et al. MRM 2001 **2)** Yacoub E et al. MRM 2001, Vaughan JT et al. MRM 2002 **3)** Collins CM et al. MRM 2001, Hoult D et al. JMRI 2000, Collins CM et al. MRM 1998, Yang Q.X. et al. MRM 2002 **4)** Adriany G et al. MRM *in press*, US Patent 6,633,161 (2003) **5)** de Zwart J.A et al. MRM 2002 **6)** Wiesinger F et al. MRM 2004

Funding: supported by: NIH- R01 EB000895, MIND Institute, KECK Foundation, NIH RR008079 *Healthy volunteers who signed a consent form approved by the University review Board